Coherent N_2^+ emission mediated by coherent Raman scattering for gas-phase thermometry

Mazza, Francesco; Buurmeijer, Hugo; Castellanos, Leonardo; Bohlin, Alexis

DOI
10.1364/OL.476540

Publication date
2022

Document Version
Final published version

Published in
Optics Letters

Letter Vol. 47, No. 23 / 1 December 2022 / Optics Letters 6105

Coherent N_2^+ emission mediated by coherent Raman scattering for gas-phase thermometry

Francesco Mazza,[1,*] Hugo Buurmeijer,[1] Leonardo Castellanos,[1] and Alexis Bohlin[1,2]

[1]Faculty of Aerospace Engineering, Delft University of Technology, Kluyverweg 1, 2629 HS Delft, The Netherlands
[2]Space Propulsion Laboratory, Department of Computer Science, Electrical and Space Engineering, Luleå University of Technology, 98128, Kiruna, Sweden
*Corresponding author: f.mazza@tudelft.nl

Received 26 September 2022; revised 20 October 2022; accepted 30 October 2022; posted 1 November 2022; published 17 November 2022

We report on the generation of coherent emission from femtosecond (fs) laser-induced filaments mediated by ultrabroadband coherent Raman scattering (CRS), and we investigate its application for high-resolution gas-phase thermometry. Broadband 35-fs, 800-nm pump pulses generate the filament through photoionization of the N_2 molecules, while narrowband picosecond (ps) pulses at 400 nm seed the fluorescent plasma medium via generation of an ultrabroadband CRS signal, resulting in a narrowband and highly spatiotemporally coherent emission at 428 nm. This emission satisfies the phase-matching for the crossed pump-probe beams geometry, and its polarization follows the CRS signal polarization. We perform spectroscopy on the coherent N_2^+ signal to investigate the rotational energy distribution of the N_2^+ ions in the excited $B^2\Sigma_u^+$ electronic state and demonstrate that the ionization mechanism of the N_2 molecules preserves the original Boltzmann distribution to within the experimental conditions tested.

https://doi.org/10.1364/OL.476540

A remarkable feature associated with femtosecond (fs) laser filamentation [1] is the generation of coherent emission from the electronically excited atomic [2] and molecular [3,4] ions in the plasma filament, both in the forward and backward directions. A number of experimental and theoretical studies have been dedicated to the coherent emission from nitrogen cations (N_2^+) [5], with particular focus on the first negative band $B^2\Sigma_u^+ \rightarrow X^2\Sigma_g^+$. Narrowband coherent emission at 391 nm and 428 nm is consistently reported, corresponding to the ro-vibronic transitions $v = 0 \rightarrow v' = 0$ and $v = 0 \rightarrow v' = 1$, respectively, with v and v' being the vibrational quantum numbers in excited and ground electronic states (Fig. 1). There is no clear consensus on the mechanism behind this "air lasing" action [5], with stimulated amplification or superradiant emission [6] from an inverted population [7,8], and lasing-without-inversion [9,10] being proposed as alternatives. Four-wave mixing and stimulated Raman scattering were rejected as amplification mechanisms on the basis of the experimental observations by Ni *et al.* in Ref. [11]. The possibility of generating an air laser remotely has potential for the development of new remote-sensing techniques of, for example, pollutants in the atmosphere [12]. Combustion researchers have recently employed filament-induced nonlinear spectroscopy to detect intermediate combustion species [13] and fs laser excitation tagging (FLEET) to measure the velocity field [14]. Filamentation has also been combined with coherent Raman scattering (CRS) for the *in situ* generation of a compressed supercontinuum to achieve ultrabroadband excitation of major combustion species [15–18], or to generate a narrowband probe pulse [19] via N_2^+ lasing. This lasing is particularly interesting for combustion diagnostics given the abundance of N_2 in air and its low chemical reactivity, and the demonstration of backward lasing from singly ionized N_2 pumped by near-infrared (IR) fs pulses [4].

In the present work, we report on air lasing mediated by CRS, whereby a filament is generated by an fs near-IR pump pulse, and the coherent N_2^+ emission at 428 nm is seeded by a narrowband picosecond (ps) probe pulse, via non-resonant (NR) CRS of the latter. The seeding mechanism observed here is clearly different from that of similar experiments, where the coherent emission results from self-seeding [20,21] or by the use of two-color collinear pump-probe schemes employing fs seed pulses, spectrally broad enough to cover the fluorescence wavelength [11,22,23]. We employ a single regenerative amplifier system (7.5 mJ, 1 kHz, Astrella Coherent) to generate the fs pump and the ps probe pulses. A 1.5-mJ portion of the broadband output of the amplifier (19.2 nm, centered at 806.7 nm) is focused through a 500-mm spherical lens to generate a ~13-mm-long filament: the pulse dispersion prior to filamentation is controlled by an external compressor unit and a residual linear chirp of ± 500 fs^2 is found to optimize the filamentation process in air [17]. The estimated pulse fluence is ~446 TW/cm^2 so that quantum tunneling is the main ionization mechanism [1]. The probe pulse is generated via second-harmonic bandwidth compression of the second 35-fs transform-limited amplifier output, producing a narrowband ~4-ps pulse (0.08 nm, centered at 403.4 nm), with 0.9 mJ/pulse [24]. The probe beam is focused through a 300-mm lens resulting in a beam diameter at the focus of ~21.5 μm ($M^2 = 1.2$), and it crosses the filament at a distance of ~5 mm from its leading edge, at an angle of ~3.5°. A delay line controls the relative delay of the two pulses, and we use polarization optics (half-wave plates and thin-film polarizers) to control the energy and polarization angle for the linear polarized pump

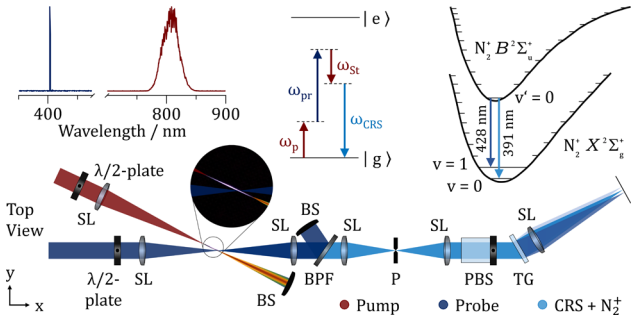

Fig. 1. Generation of air lasing mediated by NR CRS. The 1.5-mJ, ~50-fs pump pulse generates a filament, and it is compressed to ~17 fs TL [17], providing the pump (ω_p) and Stokes (ω_{St}) frequencies to the ultrabroadband CRS process; the narrowband frequency-doubled (ω_{pr}) ~4-ps probe pulse undergoes NR CRS, generating a broadband signal that seeds the fluorescent emission from the excited N_2^+. SL, spherical lens; λ/2, half-wave plate; BS, beam stop; BPF, bandpass filter; P, pinhole; PBS, polarization beam splitter; TG, transmission grating.

and probe beams before the focusing lenses. The filament emission at 428 and 391 nm has high spatial coherence and satisfies the near-phase-matching condition of the CRS process for our two-beam CRS setup [24]. This emission is collected through a polarization-sensitive coherent imaging spectrometer, dispersed by a high-density diffraction grating and imaged through a pinhole to an sCMOS camera by a 1000-mm spherical lens. A tunable bandpass filter (20-nm bandwidth, Semrock) suppresses the probe beam, nearly co-propagating with the signal. A Glan-laser polarizer acts as polarization gate to the spectrometer, allowing us to measure the polarization of the coherent N_2^+ emission.

The main features of the coherent emission generated by the fs filamentation at 428 nm are presented in Fig. 2. The role of the probe pulse in the generation of air lasing is shown in Fig. 2(a): the emission is only observed in correspondence of

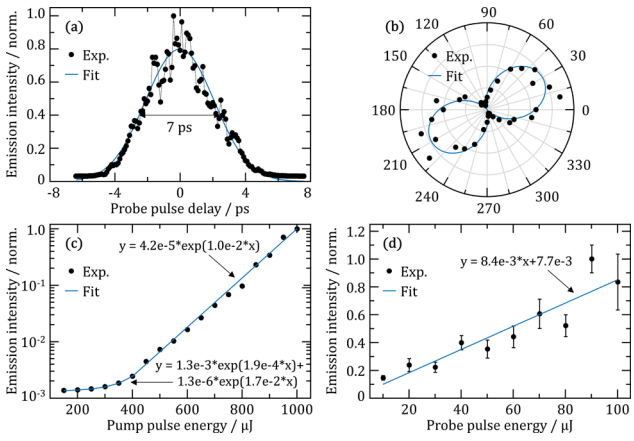

Fig. 2. Characterization of the coherent N_2^+ emission from the plasma filament. (a) Intensity of the N_2^+ emission as a function of the delay of the probe pulse relative to the pump. (b) Polarization of the N_2^+ emission (black) as a function of the probe polarization angle, and comparison with the theoretical polarization of the NR CRS signal. The pump polarization is oriented at 60° from the polarization gate in the spectrometer. (c) Power scaling of the N_2^+ emission as a function of the pump pulse energy. (d) Power scaling of the N_2^+ emission as a function of the probe pulse energy.

the temporal overlap of the pump and probe pulses. The relative arrival time of the two pulses is changed in steps of 100 fs and the resulting integrated signal maps the temporal envelope of the ps probe pulse, with a duration estimated to ~7 ps full width at half maximum (FWHM). The emission also shows high spatial coherence as it is imaged through a pinhole in the spectrometer and satisfies the phase-matching requirements of the CRS process, co-propagating with the probe beam. On the other hand, the probe pulse is off-resonant with respect to the $B^2\Sigma_u^+ \rightarrow X^2\Sigma_g^+$ro-vibronic transition, and its bandwidth is clearly too narrow to have any significant overlap with the fluorescence spectrum of N_2^+, so that it cannot directly stimulate emission from the electronically excited ions. This behavior is in contrast to the one observed by Ni *et al.*, who reported in Ref. [11] coherent emission at 391 nm with no phase-matching requirements, but only for a resonant probe pulse. We identify the reason for the peculiar behavior observed in our experiment to lie in a different seeding mechanism. The narrowband ps probe does not act directly as a seed pulse for the N_2^+ emission but undergoes four-wave mixing (NR CRS) with the ultrabroadband ~17-fs compressed supercontinuum pulse generated by filamentation. CRS thus mediates the N_2^+ emission, providing a seeding mechanism for the coherent emission at 428 nm, although this does not represent a gain mechanism alternative to those mentioned in the introduction. This process is additionally confirmed by the polarization properties of the coherent emission, as shown in Fig. 2(b). We performed a parametric study by rotating the polarization of the pump pulse relative to the polarization gate of our spectrometer from 0° to 90° in steps of 15° and, for each of these settings, we rotated the polarization of the probe pulse from 0° to 360° in steps of 10°. The experimental points (black) in the polar plot in Fig. 2(b) represents the intensity of the coherent N_2^+ emission transmitted through the polarization gate as a function of the relative probe polarization, for a pump polarization angle of 60°. The blue curve represents the theoretical behavior of the NR CRS signal as predicted by the CRS polarization theory in Ref. [17], and a similar agreement is found for all the pump polarization angles tested in our experiment. The coherent N_2^+ emission thus has the polarization of the NR CRS signal rather than that of the probe field, which confirms CRS to be the seeding mechanism, according to the experimental observations of Li *et al.*, who showed that the lasing emission is linearly polarized as the seed pulse [25].

The N_2^+ emission strongly depends on the pump pulse energy, and two distinct regimes are identified in Fig. 2(c), with a transition at ~400 μJ/pulse: for low pump energy (100–400 μJ/pulse), the emission intensity grows more than exponentially, while at larger pump energies the growth is exponential. The experimental data in the low-power regime are fitted by a linear combination of two exponential functions: this hints at two different phenomena contributing to the emission. On the one hand, the N_2^+ fluorescence has been observed to grow exponentially with the power of the pump laser [26]; on the other, the compression of the pump pulse itself grows non-linearly in the range 100–400 μJ/pulse, leading to an exponential growth of the seed power at 428 nm [16]. In contrast, the emission intensity grows linearly with the energy of the probe pulse, as shown in Fig. 2(d), in agreement with the linear scaling of the CRS signal with the probe.

The coherent emission from the filament is imaged through the spectrometer with ~1:3 magnification onto the sCMOS detector with 6.5 μm pixel-size: the multi-filament structure [1]

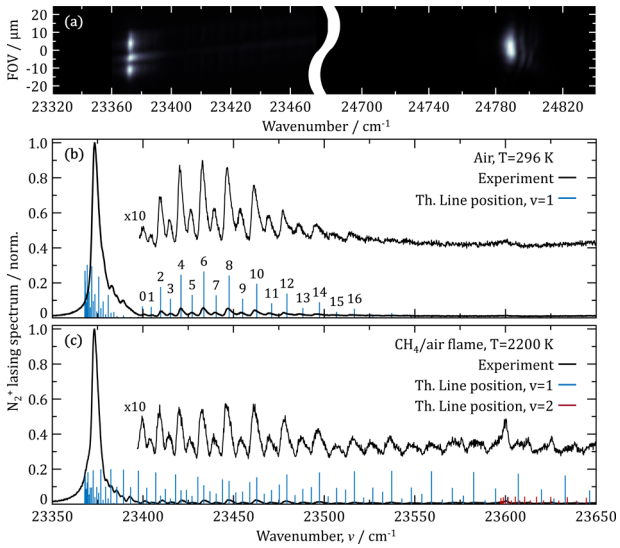

Fig. 3. Hyperspectral imaging of the coherent N_2^+ emission from the filament. (a) Multi-filament structure (on the left) as imaged by the N_2^+ emission at the probe focus (on the right). (b) Single-shot spectrum of the N_2^+ emission at 428 nm generated in air (black) and the theoretical position of the rotational lines in the fundamental vibrational band (blue). (c) Single-shot spectrum of the N_2^+ emission at 428 nm generated in a CH_4/air flame (black) and the position of the rotational lines in the fundamental (blue) and first hot (red) vibrational bands.

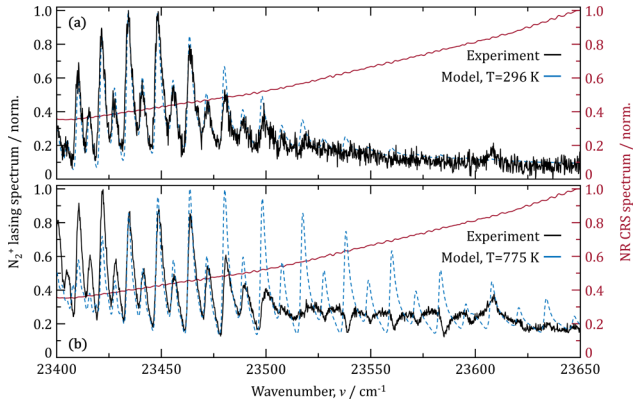

Fig. 4. Comparison of experimental N_2^+ spectra and spectral model. (a) Single-shot N_2^+ spectrum acquired in a room-temperature N_2 flow. (b) Single-shot N_2^+ spectrum acquired in a heated N_2 flow at 775 K. In red, the spectrum of the NR CRS signal acquired in argon.

of the plasma medium is visible in the imaged N_2^+ emission in Fig. 3(a). For reference, the probe beam waist is also imaged on the camera: the size of the probe at its focus was independently measured with a beam profiler (WinCam D, Dataray) to be ~21.5 µm. The diameter of the single filaments is thus estimated to be ~10 µm: this is well in agreement with the experimental results obtained by Centurion *et al.* for a 2-mJ, 150-fs near-IR pulse focused in carbon disulfide [27]. High-resolution single-shot N_2^+ spectra, acquired in room-temperature air and in the hot products of a laminar premixed methane/air flame (equivalence ratio φ=1), are shown in Figs. 3(b) and 3(c), respectively. The rotational structure of the N_2^+ emission spectrum is evident in the R-branch (23,400–23,500 cm^{-1}), where each line corresponds to the transition $N \rightarrow N-1$, with N being the nuclear angular momentum quantum number. The alternation in the intensity of adjacent lines reflects the multiplicity of triplet and heptet spin states for odd and even values of N, respectively. The P-branch ($N \rightarrow N+1$) spectrum is much more congested and gives rise to the large spectral feature at ~23,360–23,380 cm^{-1}. The spectrum acquired in the hot product gases of the flame has a much broader envelope and presents a clear feature at ~23,600 cm^{-1}: this is the vibrational hot band, corresponding to the transition $v = 2 \rightarrow v' = 1$. The change in the spectral envelope between the N_2^+ spectrum in room-temperature air and in the flame must reflect the different rotational and vibrational energy distribution of the N_2 population, according to Boltzmann statistics. This proves that, at least to a certain extent, the original ro-vibrational energy distribution is preserved in the tunneling ionization process: the N_2^+ emission spectrum could then be used for gas-phase thermometry.

We show this in Fig. 4 by comparing the experimental spectra—acquired in a flow of N_2 at room temperature and heated to 775 K (as measured by pure-rotational N_2 CRS)—and a simplified theoretical model for the emission spectrum of N_2^+. A similar model has been successfully employed by Azarm *et al.* to fit air lasing spectra at 428 nm and estimate the impact on the optical gain of different rotational energy distributions in the upper and lower electronic states [28]. The emission from the microscopic N_2^+ dipoles is treated as a coherent process by summing their contributions to the emitted field and computing the resulting intensity spectrum as the squared amplitude spectrum, in analogy to superradiant emission [29]. Additional simplifying assumptions are a homogeneous spectral density of the seeding NR CRS signal on the region 23,350–23,650 cm^{-1}, and negligible dependence on the N quantum number of the angular momenta [30] and rotational–vibrational [31] coupling in the emission process. The theoretical position of the rotational lines in the P- and R-branch spectra (ν) is converted from the energy difference between the initial ($B^2\Sigma_u^+$, v, N) and final ($X\,^2\Sigma_g^+$, v', N') ro-vibronic states of the cation:

$$\begin{aligned} \nu &= B_v N(N+1) - D_v[N(N+1)]^2 \\ \nu' &= 23392.1\ \mathrm{cm}^{-1} + B'_v N'(N'+1) - D'_v[N'(N'+1)]^2, \end{aligned} \tag{1}$$

with B_v, D_v, B'_v, and D'_v being the rotational and centrifugal constants of N_2^+ as a function of the vibrational quantum number [32]. The emission cross section is taken to be proportional to the Boltzmann distribution of the original N_2 population, thus introducing the temperature sensitivity of the N_2^+ spectrum:

$$\rho(v', N') = \exp[-\nu(v', N')\hbar c/k_B T]. \tag{2}$$

The line shape is due to interference between the N_2^+ emission and the NR CRS background, and is computed using a Fano profile [33], with resonance width $\gamma = 2.5\ \mathrm{cm}^{-1}$ and a Fano parameter of $q = 2$:

$$\Gamma = \frac{(q\gamma/2 + \omega - \nu)^2}{(\gamma/2)^2 + (\omega - \nu)^2}. \tag{3}$$

The comparison between the experimental spectra and the theoretical model is somewhat complicated by the presence of the NR CRS, which on the one hand acts as a seed for the N_2^+ emission, but on the other is a background to its spectrum. The interference between the N_2^+ spectrum and the NR background results in a distortion of the spectral envelopes in Fig. 4. This is particularly significant at larger wavenumbers, where the intensity

of the rotational lines of the N_2^+ spectrum is reduced according to their Boltzmann population, while the NR background grows for reducing Raman shifts with respect to the probe line at 24,790 cm^{-1}, as shown in Fig. 4. The room-temperature spectrum in Fig. 4(a) is almost unaffected by the presence of the background and shows a good agreement with the theoretical model. In Fig. 4(b), higher rotational lines are populated at 775 K, giving rise to interference with the NR background: this completely suppresses line R(16) at ~23,517 cm^{-1}, and the following lines are identified with the negative peaks in the continuous background.

In conclusion, we reported the observation of air lasing from a filament generated by near-IR fs pulses, mediated by NR CRS as the seeding mechanism. The dynamics of the seeding process are demonstrated by the phase-matching of the coherent emission from the filament, according to the crossing angle of the narrowband ps probe beam, and by its polarization dependence on the linearly polarized pump and probe pulses. We investigated the temperature dependence of the coherent emission from excited N_2^+ and recording single-shot spectra in air, a heated N_2 flow, and in a laminar CH_4/air flame. The N_2^+ spectrum shows a clear temperature dependence, which points to an isothermal population transfer from N_2 to N_2^+ in the tunneling ionization regime. The experimental spectra are compared to a simple spectral model: a good agreement is shown at room temperature, while the interference between the N_2^+ emission and the NR CRS seed suppresses higher rotational lines in the spectrum of the former, severely skewing the spectral envelope at greater temperatures. Modelling of the NR CRS spectrum or background suppression schemes could improve the quantitative comparison and lead to the development of air lasing thermometry (ALT) as a robust diagnostics technique, with potential for remote sensing and single-ended optical probing, as well as for spatial resolution below the diffraction limit. Future work should address questions about the impact of the ionization efficiency [34] on the ro-vibrational energy distribution of N_2^+, the possible rotational non-equilibrium in inverted population systems [28], as well as the effect of rotational wave packets created by stimulated Raman scattering [35], and incorporate these in the spectral model for the coherent N_2^+ emission.

Funding. Nederlandse Organisatie voor Wetenschappelijk Onderzoek (AES-15690).

Acknowledgments. We gratefully acknowledge the financial support provided by the Netherlands Organization for Scientific Research (NWO). A. Bohlin is thankful for support through the RIT (Space for Innovation and Growth) project/European Regional Development Fond in Kiruna, Sweden.

Disclosures. The authors declare no conflicts of interest.

Data availability. Data underlying the results presented in this paper are not publicly available at this time but may be obtained from the authors upon reasonable request.

REFERENCES

1. A. Couairon and A. Mysyrowicz, Phys. Rep. **441**, 47 (2007).
2. A. Dogariu, J. B. Michael, M. O. Scully, and R. B. Miles, Science **331**, 442 (2011).
3. S. Mitryukovskiy, Y. Liu, P. Ding, A. Houard, and A. Mysyrowicz, Opt. Express **22**, 12750 (2014).
4. X. Zhang, R. Danylo, Z. Fan, P. Ding, C. Kou, and Q. Liang, Appl. Phys. B **126**, 53 (2020).
5. P. Polynkin and Y. Chen, *Air Lasing*, 1st ed. (Springer International Publishing, 2018).
6. Y. Liu, P. Ding, G. Lambert, A. Houard, V. Tikhonchuk, and A. Mysyrowicz, Phys. Rev. Lett. **115**, 133203 (2015).
7. H. Xu, E. Lötstedt, A. Iwasaki, and K. Yamanouchi, Nat. Commun. **6**, 8347 (2015).
8. J. Yao, S. Jiang, W. Chu, B. Zeng, C. Wu, R. Lu, Z. Li, H. Xie, G. Li, C. Yu, Z. Wang, H. Jiang, Q. Gong, and Y. Cheng, Phys. Rev. Lett. **116**, 143007 (2016).
9. A. Mysyrowicz, R. Danylo, A. Houard, V. Tikhonchuk, X. Zhang, Z. Fan, Q. Liang, S. Zhuang, L. Yuan, and Y. Liu, APL Photonics **4**, 110807 (2019).
10. M. Richter, M. Lytova, F. Morales, S. Haessler, O. Smirnova, M. Spanner, and M. Ivanov, Optica **7**, 586 (2020).
11. J. Ni, W. Chu, C. Jing, H. Zhang, B. Zeng, J. Yao, G. Li, H. Xie, C. Zhang, H. Xu, S.-L. Chin, Y. Cheng, and Z. Xu, Opt. Express **21**, 8746 (2013).
12. P. R. Hemmer, R. B. Miles, P. Polynkin, T. Siebert, A. V. Sokolov, P. Sprangle, and M. O. Scully, Proc. Natl. Acad. Sci. U. S. A. **108**, 3130 (2011).
13. H.-L. Li, H.-L. Xu, B.-S. Yang, Q.-D. Chen, T. Zhang, and H.-B. Sun, Opt. Lett. **38**, 1250 (2013).
14. J. B. Michael, M. R. Edwards, A. Dogariu, and R. B. Miles, Appl. Opt. **50**, 5158 (2011).
15. J. H. Odhner, D. A. Romanov, and R. J. Levis, Phys. Rev. Lett. **103**, 075005 (2009).
16. F. Mazza, N. Griffioen, L. Castellanos, D. Kliukin, and A. Bohlin, Combust. Flame **237**, 111738 (2022).
17. F. Mazza, A. Stutvoet, L. Castellanos, D. Kliukin, and A. Bohlin, Opt. Express **30**, 35232 (2022).
18. Z. Tian, H. Zhao, Y. Gao, H. Wei, Y. Tan, and Y. Li, Appl. Phys. Lett. **121**, 081102 (2022).
19. X. Zhao, S. Nolte, and R. Ackermann, Opt. Lett. **45**, 3661 (2020).
20. T. J. Wang, J. Ju, J. F. Daigle, S. Yuan, R. Li, and S. L. Chin, Laser Phys. Lett. **10**, 125401 (2013).
21. Y. Liu, Y. Brelet, G. Point, A. Houard, and A. Mysyrowicz, Opt. Express **21**, 22791 (2013).
22. J. Yao, G. Li, C. Jing, B. Zeng, W. Chu, J. Ni, H. Zhang, H. Xie, C. Zhang, H. Li, H. Xu, S. L. Chin, Y. Cheng, and Z. Xu, New J. Phys. **15**, 023046 (2013).
23. Y. Fu, E. Lötstedt, H. Li, S. Wang, D. Yao, T. Ando, A. Iwasaki, F. H. M. Faisal, K. Yamanouchi, and H. Xu, Phys. Rev. Res. **2**, 012007 (2020).
24. L. Castellanos, F. Mazza, D. Kliukin, and A. Bohlin, Opt. Lett. **45**, 4662 (2020).
25. H. Li, Q. Song, J. Yao, Z. Liu, J. Chen, B. Xu, K. Lin, J. Qiang, B. He, H. Xu, Y. Cheng, H. Zeng, and J. Wu, Phys. Rev. A **99**, 053413 (2019).
26. Q. Luo, W. Liu, and S. L. Chin, Appl. Phys. B **76**, 337 (2003).
27. M. Centurion, Y. Pu, M. Tsang, and D. Psaltis, Phys. Rev. A **71**, 063811 (2005).
28. A. Azarm, P. Corkum, and P. Polynkin, Phys. Rev. A **96**, 051401 (2017).
29. M. Gross and S. Haroche, Phys. Rep. **93**, 301 (1982).
30. H. Hönl and F. London, Z. Physik **35**, 286 (1926).
31. R. Herman and R. F. Wallis, J. Mol. Spectrosc. **2**, 369 (1958).
32. R. R. Laher and F. R. Gilmore, J. Phys. Chem. Ref. Data **20**, 685 (1991).
33. U. Fano, Phys. Rev. **124**, 1866 (1961).
34. I. V. Litvinyuk, K. F. Lee, P. W. Dooley, D. M. Rayner, D. M. Villeneuve, and P. B. Corkum, Phys. Rev. Lett. **90**, 233003 (2003).
35. H. Xie, B. Zeng, G. Li, W. Chu, H. Zhang, C. Jing, J. Yao, J. Ni, Z. Wang, Z. Li, and Y. Cheng, Phys. Rev. A **90**, 042504 (2014).